11th CIRP Conference on Intelligent Computation in Manufacturing Engineering - CIRP ICME '17

Effects of Lubrication on Friction and Heat Transfer in Machining Processes on the Nanoscale: A Molecular Dynamics Approach

Martin P. Lautenschlaeger[a*], Simon Stephan[a], Martin T. Horsch[a], Benjamin Kirsch[b], Jan C. Aurich[b], Hans Hasse[a]

[a]Laboratory of Engineering Thermodynamics (LTD), University of Kaiserslautern, 67663 Kaiserslautern, Germany
[b]Institute for Manufacturing Technology and Production Systems (FBK), University of Kaiserslautern, 67663 Kaiserslautern, Germany
Fehler! Textmarke nicht definiert.

* Corresponding author. Tel.: +49-631-205-2132; fax: +49-631-205-3835. *E-mail address:* Martin.Lautenschlaeger@mv.uni-kl.de

Abstract

Working fluids play an important role in machining processes. They have two primary tasks: On the one hand, they reduce the friction and thus weaken the generation of heat in the machining process. On the other hand, the working fluid cools the workpiece and the tool acting as a heat sink. Both functionalities are investigated in the present work by means of molecular dynamics simulations of nanometric machining processes. The action of the tip of a cutting tool on a workpiece is investigated both with and without working fluid. The Lennard-Jones truncated and shifted model is used for describing all occurring atomic interactions. The simulation results show that even in the presence of the liquid working fluid, the tool and the workpiece are mostly in direct contact during the machining process, i.e. the initially present fluid particles are squeezed out of the contact zone. The work that is needed for the nanometric machining process is not reduced by the fluid, but the coefficient of friction is. The latter results from a reduction of the normal force acting on the cutting tool which is needed for realizing the prescribed path of the tool. As expected, the working fluid has an important influence on the thermal regime during the nanometric machining process. Both the thermal and the mechanical effects are shown to depend significantly on the solid-fluid interaction energy. The results give insight in nanoscale phenomena in the contact zone between the tip of a cutting tool and the workpiece, that cannot be studied experimentally.

Keywords: Cutting, Grinding, Friction, Indentation, Lubricant, Dissipation, Molecular Dynamics Simulation, Solid-Fluid Interface

1. Introduction

The small zone in which the cutting tool and the workpiece are in direct contact in machining processes is hard to study experimentally, so that up to now there is only little information on the phenomena which occur in that highly important zone. Molecular dynamics simulations are an attractive way for providing such information. While molecular dynamics simulations of microscale objects have already been carried out [X1], system sizes which are accessible by simulations are typically on the nanoscale.

The nanoscale is also becoming directly relevant for modern micro and precision machining technology. E.g. in manufacturing of optical and photonic products tolerances in the order of nanometers must be met [1]. Processes on the nanoscale can be governed by different effects compared to the corresponding processes on larger scales. It is e.g. well known from studies of fluid flow, that on small scales interfacial effects, which are negligible on larger scales become dominant [18].

In molecular dynamics simulations Newton's equations of motion are solved for an atomistic many-particle system. The interactions of the particles are described by classical force fields. For a given force field, only the scenario which is to be studied has to be specified. There are no assumptions or parameters, so that the simulation is completely predictive. Due to the strong physical background of the method, molecular dynamics simulations are often used in situations in

where the predictive power matters [ZITAT, MARTIN H. KANN BESTIMMT EINS LIEFERN].

Molecular dynamics simulations have been used since the late 1980s [28] for studying tool-workpiece interactions. However, in most of these studies only the dry contact was studied, i.e. the tool and the workpiece interacted in a vacuum; see e.g. [2–7]. The focus of these studies was on the chip formation and the generation of dislocations in the workpiece.

It is, however, well known from macroscopic studies that machining processes are significantly influenced by cooling and lubrication due to working fluids [8, 9]. There are up to now only a few molecular simulation studies which have addressed this [1, 10–14]. In these studies, typically a single substrate-fluid pair is investigated, and no special attention is given to the influence of the substrate-fluid interaction, even though that interaction is known to play a predominant role in closely related processes like wetting [15, 16]. Furthermore, the thermal effects are usually not in the focus of the available studies. Therefore, in the present work, a molecular dynamics study of the effect of the working fluid on nanometric machining processes was carried out using a model system that enables systematic studies of the influence of the substrate-fluid interaction ε_{SF}. Here, both the mechanical and the thermal effects of the working fluid were studied by comparison to the dry case. Additional information on the mechanical effects is available in [LAUTENSCHLAEGER IRTG].

2. Modeling and Simulation Setup

2.1. Molecular Model

The studied system consists of a workpiece, i.e. a solid substrate (S), the tip of a cutting tool (T), and eventually the working fluid (F). The tip is rigid, its movement is prescribed. All interactions are modeled with the Lennard-Jones truncated and shifted (LJTS) potential $u^{LJTS}(r_{ij})$, i.e. those between the alike sites S-S and F-F, as well as the unlike interactions S-F, T-F, and S-T. The LJTS model is well suited for describing properties of simple non-polar fluids [17, 18], but it is only a crude model for solids. We use it throughout because we carry out a study of basic effects for which simplicity is beneficial. Furthermore, we can build on a recent study of the wetting behavior of LJTS walls by LJTS fluids [15, HIER KÖNNTE NOCH EINE NEUE ARBEIT DAZUKOMMEN, DIE GERADE IM REBUTTAL IST, WIR SOLLTEN DAS SPÄTER GGF ERGÄNZEN].

The LJTS potential is [ZITAT]:

$$u^{LJTS}(r_{ij}) = \begin{cases} u^{LJ}(r_{ij}) - u^{LJ}(r_c), & r_{ij} < r_c \\ 0, & r_{ij} \geq r_c \end{cases}, \quad (1)$$

where

$$u^{LJ}(r_{ij}) = 4\varepsilon[(\sigma / r_{ij})^{12} - (\sigma / r_{ij})^6], \quad (2)$$

Here, ε is the energy parameter, describing dispersive attraction, σ is the size parameter describing the repulsion. r_{ij} is the distance between two LJTS sites i and j, and r_C is the cut-off radius, which is the maximal distance for which the attraction is considered.

The parameterization which is presented below results from preliminary test runs with different parameterizations. In follow-up work systematic parameter variations will be carried out.

The specific parameterization of the LJTS interactions in that study was chosen to mimic a system containing argon [23] or methane for the fluid and a common metal like iron or vanadium for the substrate [19]. All sites have the same mass M. The size parameter σ is used to normalize all distances. Moreover, σ is the same for all LJTS sites. The cut-off radii of all alike and unlike interactions are 2.5σ, except of the substrate-tool interaction, that was kept purely repulsive by setting its cut-off to $r_{C,ST} = 1.0\sigma$, cf. [20]. All energies are normalized using the LJTS energy parameter of the fluid $\varepsilon = \varepsilon_F$. The cohesive energy of the substrate is set to $\varepsilon_S = 52\ \varepsilon_F$. For the substrate-fluid and the tool-fluid interactions the cohesive energy is $\varepsilon_{SF} = \varepsilon_{TF} = 0.5\ \varepsilon_F$. According to *Becker et al.* [15], the latter interaction energies correspond to a contact angle of about 90°. In follow-up work a systematic variation of the contact angle will be carried out.

All observables presented in that work are given in reduced units, cf. Table 1. Here, k_B is the Boltzmann's constant.

Table 1. Characteristic system properties in quantities carrying dimensions.

Length	$x = x^* / \sigma$
Time	$\tau = \tau^* / \left(\sigma\sqrt{M / \varepsilon}\right)$
Mass	$m = m^* / M$
Temperature	$T = T^* / (\varepsilon / k_B)$
Pressure	$p = p^* / (\varepsilon / \sigma^3)$
Velocity	$v = v^* / \left(\sqrt{\varepsilon / M}\right)$
Force	$F = F^* / (\varepsilon / \sigma)$
Work	$W = W^* / \varepsilon$
Thermal conductivity	$\lambda = \lambda^* / \left(k_B / \left(\sigma^2 \sqrt{M / \varepsilon}\right)\right)$

2.2. Simulation Scenario

In the present scenario the physical phenomena at the tip of a cutting tool and in its close vicinity are investigated. Therefore, a solid cylinder, modeling the cutting edge of the cutting tool, firstly penetrates the substrate and then is laterally scratched over the substrate surface. The entire simulation box has the dimensions $l_x = 309$, $l_y = 71$ and $l_z = 295$. For the lubricated case it includes a total number of $4.89 \cdot 10^6$ LJTS sites that are assigned to the substrate $(3.16 \cdot 10^6)$, the cutting tool $(1.67 \cdot 10^4)$, and the fluid $(1.71 \cdot 10^6)$, respectively. A detail of the entire simulation box for the lubricated case is depicted in Fig. 1. Here, a two-dimensional projection of the three-dimensional rigid cutting edge with the radius $R = 9$ and the length $L = 71$ is shown. Due to Fig. 1 the origin of x indicates the initial position of the rotational axis of the cylinder, which is constant during the indentation. The origin of z indicates its position when the

distance between the rotational axis of the cutting tool and the initially flat substrate surface is equivalent to the cylinder's radius R. In the initial situation, the substrate is a crystal with a fcc lattice and the particle density $\rho = 1.07$.

Due to the two-dimensional projection of the three-dimensional system, periodic boundary conditions are applied for all components in all dimensions, except for the fluid where in z-direction a soft repulsive boundary condition is used. The two layers of substrate sites next to the box margins in *x*-direction and at the bottom of the box are fixed. Additionally, three layers of a velocity scaling thermostat are deposited next to the fixed layers keeping the temperature at $T = 0.8$ throughout the entire simulation. That temperature is equivalent with the initial temperature of the system after the equilibration. The initial pressure is $p = 0.005$. During the whole process, no evaporation is observed for the fluid, i.e. it is entirely liquid.

The kinetic process of the cutting tool is subdivided into the indentation in negative *z*-direction, where the cutting tool penetrates the substrate until its rotational axis has reached the position $z = -4.5$. Thereafter, a scratching in *x*-direction at constant z is performed. The total covered distance is $d = 45$. It is assigned to an indentation length of 10, and a scratching length of 35. The speed of the cutting tool is $v = 0.12$ for both movements. The time step applied for the simulations is $\Delta\tau = 0.006$. All simulations were carried out using LAMMPS [21].
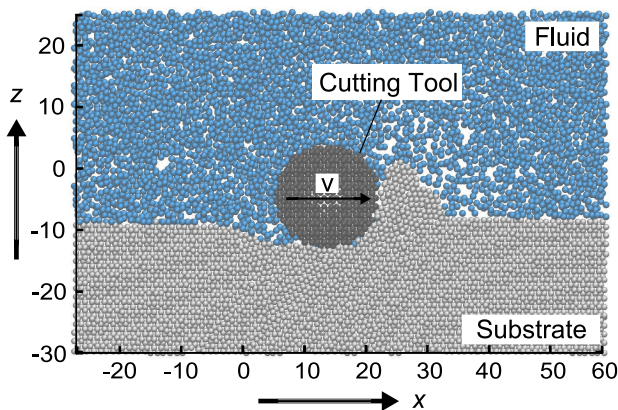
Fig. 1. Schematic depiction of the simulation scenario.

3. Simulation Results

A snapshot of a simulation considering a fluid is shown in Fig. 1. It depicts the molecular setup after half of the scratching length. It is obvious, that there is a pile-up of material in front of the cutting tool, i.e. a chip is formed. Also the stacking faults in the substrate are visible. Besides, as only a thin slice in *y*-direction is shown, the lowering of the density of the fluid in the vicinity of the chip, where the temperature is high, can be seen. One of the most striking features of the simulation is that there are hardly any fluid particles in the contact zone between the cutting tool and the substrate. That phenomenon has already been observed by *Rentsch et al.* [10] as well as by *Childs* [22], who reports that for scratching

velocities of the order of m/s the stresses in the contact zone are too high for the fluid to penetrate into it.

To illustrate the results, which are presented in dimensionless variables in that work, Table 2 contains some of the key properties transformed to variables carrying dimensions. For that purpose, the LJTS parameters of argon as reported by *Vrabec et al.* [23] were used.

Table 2. Characteristic system properties in quantities carrying dimensions.

Observable	Real unit	
System size	$105 \cdot 24 \cdot 100$	nm³
Time step	1.2	fs
Initial pressure	$2.4 \cdot 10^5$	N/m²
Initial temperature	110.3	K
Substrate density	1.82	g/cm³
Cutting tool radius	3.0	nm
Indentation depth	1.5	nm
Cutting tool velocity	20.0	m/s
Total covered distance	15.2	nm

3.1. Mechanical Phenomena

For the mechanical behavior of the system mainly the total forces acting on the cutting tool and directly related quantities during the process are studied. Comparing the dry and the lubricated case we find that they differ only slightly. Representative for the more detailed study of the mechanical properties [IRTG Paper] we discuss here the accumulated work conducted by the cutting tool W_T. It is calculated as the integral of the forces for the covered distance d. In Fig. 2 it is depicted for both the dry case (black line) and the lubricated case (blue line) in dependence on the total covered distance d. Here, the two different phases of the movement can be distinguished easily by means of the profiles. Firstly, the indentation is represented for $d \in [0; 10]$. During that phase the differences between the dry and the lubricated case are minor but systematical. Here, for the lubricated case W_T is higher compared with the dry case. That is a consequence of the influence of the adsorbed fluid layer on the surface. In other words, here, the counterforce opposed by the fluid's viscosity becomes discernible. This is in line with the results of *Vo et al.* [24].

For the scratching ($d \in [10; 45]$), especially at the beginning of that phase ($d \in [10; 20]$), we find the most striking differences between both cases. Here, the rise of W_T is faster for the dry case than for the lubricated case. The reason is that fluid atoms have to be squeezed out of the contact zone, which leads to a dampening effect in the lubricated case, cf. [22]. In the following process there are no significant differences between both cases. The majority of the conducted work W_T is due to the influence of lattice deformations in the substrate. Thus, it is not affected by the lubrication.

To transfer our findings observed on scratching length of nanometers to a more continuous machining process, we average all mechanical observables during the steady state, i.e. for $d \in [20; 45]$. That corresponds to an averaging over

350,000 time steps. The results are summarized in Table 3. Here, especially the coefficient of friction (COF) is found to be slightly lower for the lubricated case. That is mainly due to the higher magnitude of the force acting on the cutting tool in z-direction. *Chen et al.* [12] also found a decrease of the COF
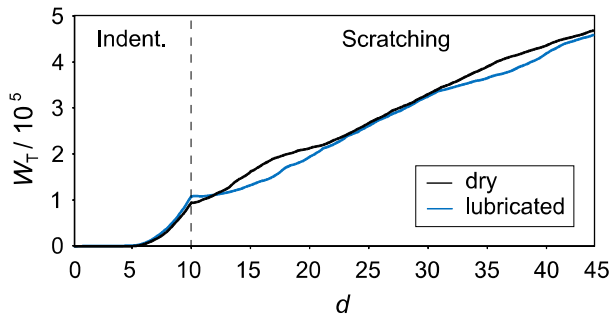
Fig. 2. Work conducted by the cutting tool: dry (black) vs. lubricated (blue).

for lubricated scenarios due to the same reason. Besides, the lubrication has an effect on the surface structure (cf. Table 3). For a detailed insight and a discussion of the mechanical properties and the surface structure we refer to *Lautenschlaeger et al.* [IRTG Paper].

3.2. Thermophysical Phenomena

Up to now, we showed that the difference of W_T for both cases is about 4 % for the steady state and only 2 % for the total process (cf. Fig. 2). Thus, it is not significant taking into account for the high fluctuations of the forces acting on the cutting tool (cf. [IRTG Paper]). Therefore, we conclude that the energy input, in terms of the work, and thus, the dissipation is equivalent for both the dry and the lubricated case. Moreover, since, there is hardly any fluid in the major area of dissipation, i.e. the substrate-tool contact zone, the principal path of the heat transport is the same in both scenarios. The heat firstly has to be transferred through the substrate, i.e. mainly the chip. Therefore, all differences regarding the heat balance of the two systems are directly related to the lubrication in the vicinity of the substrate and coherent substrate-fluid interfacial effects.

Following that argumentation, we now discuss the thermophysical behavior of the system. Therefore, in Fig. 3 the temperature distribution is shown comparing both the dry (Fig. 3a) and the lubricated (Fig. 3b) case. Here, just a detail of the entire simulation box containing the most prominent temperature gradients is depicted. The record was taken at the end of the scratching process. Of particular note is, that although, the mechanical response in both scenarios (cf. Table 3) differs only slightly in the steady state, that is not the case for the thermal response.

Again, regarding Fig. 3, it is obvious that the chip temperature is higher for the dry case. Since, there is no heat flux to the vacuum, the energy accumulates in the chip. That leads to a maximum chip temperature of $T = 2.83$ for the dry case, while the maximum chip temperature is $T = 2.10$ for the lubricated case. Due to the averaging and binning for the temperature calculation both temperature values should be

considered rather qualitatively as a ratio between the dry and the lubricated case. However, *Chen et al.* [11, 12] describe a similar temperature development in the substrate, where the highest temperature occurs in the chip under dry machining. Therefore, we state that the task of the fluid as a heat sink, in the sense of the heat balance, is remarkable.

Table 3. Comparison of relevant mechanical and structural observables.

	Dry	Lubricated
Force in z-direction	$1.17 \cdot 10^5$	$1.42 \cdot 10^5$
Force in –x-direction	$1.22 \cdot 10^5$	$1.27 \cdot 10^5$
Coefficient of friction	1.04	0.90
Scratching work	$30.5 \cdot 10^5$	$31.7 \cdot 10^5$
Relative surface enlargement	14 %	7 %
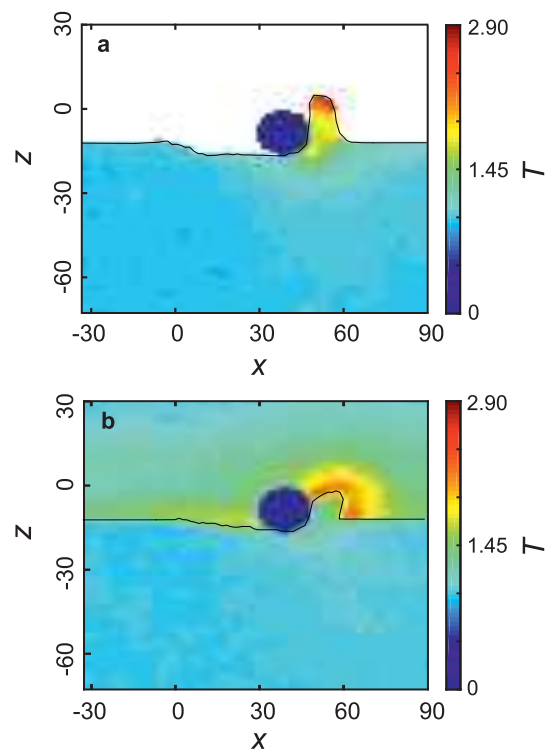
Fig. 3. Temperature field for (a) the dry case; (b) the lubricated case.

Notice, that those findings differ fundamentally from those of *Rentsch et al.* [10], where the chip temperature increased drastically for the lubricated scenario. Thereby, the fluid was thermostated throughout the simulation, whereas in ours the temperature was controlled just in single substrate layers at the bottom and lateral margins of the simulation box.

That fact can be substantiated considering Fig. 4. Here, the development of the average temperature of the fluid during the entire process is depicted with the black line. At the end of the indentation (cf. $d \in [6.7; 10]$) the temperature decreases slightly, which might be an artefact of the method of the temperature calculation. The latter is strongly dependent on the correct separation of the thermal kinetic energy and the kinetic energy due to directed velocities, i.e. the macroscopic flow. That separation might be impeded due to the unsteady flow behavior during the squeeze out of the fluid from the contact zone. However, during the scratching phase, that

artefact is not influential anymore, since the flow behavior is more regular. Here, the temperature increases continuously with an almost uniform gradient from $T = 0.8$ to $T = 0.95$. We point out, that from a macroscopic point of view that steep temperature increase in the fluid seems unrealistic. Notice that in the present scenario the volume of the fluid is in the order of 1.0e-22 m³ and thus, the average value of the fluid temperature heats up very fast. Therefore, a less biased measure for the same statement is the ratio of the gain of internal energy of the fluid U_T to the dissipation energy W_T. In Fig. 4 the gain of internal energy is depicted with the blue line. Since it is proportional to the temperature increase in the fluid, its gradient is uniform during the scratching phase, too. Comparing the final value of the internal energy of the fluid U_F with that of the total work of the cutting tool W_T yields that 11.2 % of the dissipative energy is absorbed by the fluid. That is a remarkable proportion and underpins the thermal influence of fluids as a heat sink during nanometric machining processes.

The previous finding can be explained by a superposition of several, partly nanoscale specific influence factors. One is known as the Kapitza effect, which is an additional influence factor when investigating heat transfer on the nanoscale. Here, a heat flow $\dot{q}$ over an interface is accompanied by an unsteady temperature jump ΔT. That was discovered by *Kapitza* [29] and usually is formulated as

$$\dot{q} = \frac{\Delta T}{R_K}, \tag{3}$$

and can be linked to another relation

$$\Delta T = L_K \frac{\partial T}{\partial n}. \tag{4}$$

Here, R_K is the Kapitza resistance, L_K is the Kapitza length. $\partial T / \partial n$ is the temperature gradient in the fluid in the normal direction due to the substrate surface at the interface. The Kapitza resistance is due to inhibited momentum transfer through the interface for the sole phonon transfer mechanism. The momentum transfer is strongly influenced by the strength of the unlike interactions at the interface. That relation has been shown by *Kim et al.* [30] and *Vo et al.* [24], who state that L_K decreases with an increasing solid-fluid interaction energy $\varepsilon_{\text{Interface}}$. Thereby, taking into account Eq. (3) and Eq. (4), R_K decreases with increasing $\varepsilon_{\text{Interface}}$, since the temperature gradient increases with increasing $\varepsilon_{\text{Interface}}$ [31]. Moreover, *Shi et al.* [31] and *Kim et al.* [24] show that with increasing temperature of the solid substrate L_K and thereby R_K increase. [33]

In our results, those correlations just apply for the lubricated case. Here, those effects seem to superpose and might yield a higher fluid temperature and a faster fluid temperature increase, respectively, for a higher $\varepsilon_{\text{Interface}}$. That is going to be investigated in detail in follow-up studies.

However, the heat transport originating from the contact zone is not just dependent on the thermal resistance at the interface, but also on the thermal conductivities λ of both the
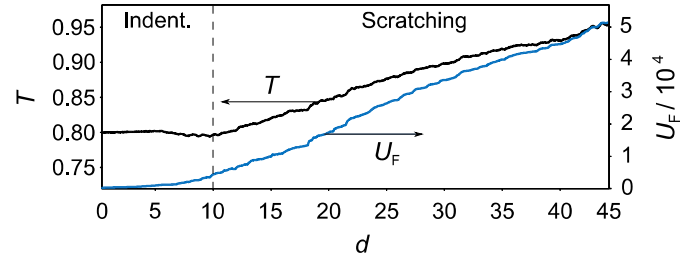
Fig. 4. Average fluid temperature (black) and fluid's internal energy (blue).
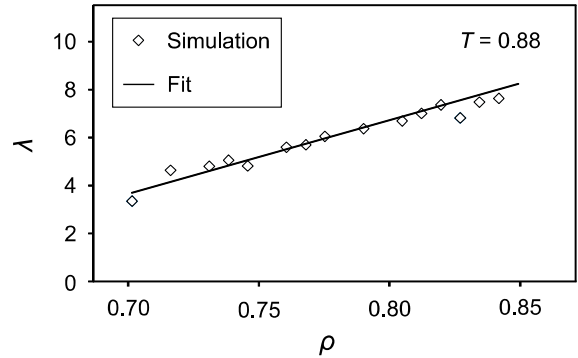
Fig. 5. Density dependence of the thermal conductivity of liquid argon.

substrate and the fluid. On the one hand, the bulk values have to be taken into account. Notice, for the solid substrate, due to the LJTS potential, the thermal conductivity is insufficiently described by the simple phonon-like atom-atom interaction. That leads to a low thermal conductivity and thus, steep temperature gradients in the solid [32]. Nevertheless, in the considered temperature range, it does rarely depend on the bulk temperature [10]. In contrast, the fluid, also regarding its thermal conductivity, is well described by the LJTS potential. According to our investigations about transport coefficients and the literature (cf. [26,27]), the fluid's thermal conductivity is strongly dependent on the temperature and is known to decrease with an increasing fluid temperature.

Moreover, the dependency of the thermal conductivity on the density at a constant temperature is significant, too. Fig. 5 shows such a correlation for the temperature $T = 0.88$. Here, the hollow hashes depict the results gained via the Green-Kubo method, while the black line shows the trend of the correlation. Notice, that e.g. at the constant temperature $T = 0.88$ increasing the density of the fluid about 25 % leads to a doubling of the thermal conductivity.

Regarding our study, that has an impact for the heat flux in the lubricated case. Here, the density of the adsorbed fluid layers close to the substrate surface is higher than in the bulk. That results in a steep increase in the thermal conductivity in the adsorbed layers. Finally, that supports the heat flux in the direction tangential to the surface, accelerates the cooling of the contact zone and results in a faster heating up of the fluid.

4. Conclusion

In the present work, the method of molecular dynamics simulations has been applied to study the influence of

lubrication on a nanometric machining process. The process' kinematics was implemented via a cutting tool firstly penetrating a solid substrate vertically, and subsequently scratching the surface horizontally. The two scenarios that were studied included a dry case and a lubricated case. Here, for the latter, the substrate and the cutting tool are immersed in a fluid. All components are modeled by LJTS potentials regarding their atomic interactions. Due to the parametrization, the system mimics liquid argon as the fluid interacting with vanadium as the substrate.

For the given solid-fluid interaction we find, that there is hardly any fluid in the contact zone between the cutting tool and the substrate. Therefore, comparing the dry and the lubricated case with respect to the mechanical properties yields minor differences. The coefficient of friction is slightly reduced in the lubricated case. However, the lateral forces and the dissipation are equivalent.

For the thermal system behavior the impact of the fluid in the sense of a heat sink is remarkable. About 11.2 % of the dissipative energy is absorbed into the fluid. We show, as per the literature, that value is strongly dependent on different interfacial effects that are mainly influenced by the solid-fluid interaction energy. However, here, only a single parameter combination was considered.

Therefore, the present work should be treated as a case study. We present a setting, which is useful to study lubricated nanometric machining regarding it mechanical and thermophysical behavior. That way is shown to be feasible and to yield interesting results. Systematic studies with comprehensive parameter variations and analysis are going to be the topic of future work of our group.

Acknowledgements

References

[1] Goel, S. ; Luo, X. ; Agrawal, A. ; Reuben, R.: Diamond Machining of Silicon: A Review of Advances in Molecular Dynamics Simulation. In: Int. J. Mach. Tool and Manuf. 88 (2015), S. 131–164

[2] Gao, Y. ; Urbassek, H.: Evolution of plasticity in nanometric cutting of Fe single crystals. In: Applied Surface Science 317 (2014), S. 6–10

[3] Aristizibal, H. ; Parra, P. ; López, P. ; Restrepo-Parra, E.: Atomistic-Scale Simulations of Material Behaviors and Tribology Properties for BCC Metal Films. In: Chin. Phys. B 25 (2016), S. 010204

[4] Cho, M. ; Kim, S. ; Lim, D. ; Jang, H.: Atomistic Scale Stick-Slip Caused by Dislocation Nucleation and Propagation During Scratching of a Cu Substrate With a Nanoindenter: A Molecular Dynamics Simulation. In: Wear 259 (2005), S. 1392–1399

[5] Gao, Y. ; Lu, C. ; Huynh, N. ; Michal, G. ; Zhu, H. ; Tieu, A.: Molecular Dynamics Simulation of Effect of Indenter Shape on Nanoscratch of Ni. In: Wear 267 (2009), S. 1998–2002

[6] Wu, C. ; Fang, T. ; Lin, J.: Atomic-scale Simulations of Material Behaviors and Tribology Properties for FCC and BCC Metal Films. In: Material Letters 80 (2012), S. 59–62

[7] Zhang, L. ; Zhao, H. ; Yang, Y. ; Huang, H. ; Ma, Z. ; Shao, M.: Evaluation of Repeated Singlepoint Diamond Turning on the Deformation Behavior of Monocrystalline Silicon via Molecular Dynamic Simulations. In: Applied Physics A 116 (2014), S. 141–150

[8] Brinksmeier, E. ; Heinzel, C. ; Wittmann, M.: Friction, Cooling and Lubrication in Grinding. In: CIRP Annals - Manufacturing Technology 48 (1999), S. 581–598

[9] Brinksmeier, E. ; Meyer, D. ; Huesmann-Cordes, A. ; Herrmann, C.: Metalworking Fluids - Mechanisms and Performance. In: CIRP Annals - Manufacturing Technology 64 (2015), S. 605–628

[10] Rentsch, R. ; Inasaki, I.: Effects of Fluids on the Surface Generation in Material Removal Processes - Molecular Dynamics Simulation -. In: Annals of the CIRP 55 (2006), S. 601–604

[11] Chen, R. ; Liang, M. ; Luo, J. ; Lei, H. ; Guo, D. ; Hu, X.: Comparison of Surface Damage Under the Dry and Wet Impact: Molecular Dynamics Simulation. In: Applied Surface Science 258 (2011), S. 1756–1761

[12] Chen, Y. ; Han, H. ; Fang, F. ; Hu, X.: MD Simulation of Nanometric Cutting of Copper With and Without Water Lubrication. In: Science China 57 (2014), S. 1154–1159

[13] Ren, J. ; Zhao, J. ; Dong, Z. ; Liu, P.: Molecular Dynamics Study on the Mechanism of AFMbased Nanoscratching Process With Water-layer Lubrication. In: Applied Surface Science 346 (2015), S. 84–98

[14] Tang, C. ; Zhang, L.: A Molecular Dynamics Analysis of the Mechanical Effect of Water on the Deformation of Silicon Monocrystals Subjected to Nano-Indentation. In: Nanotechnology 16 (2005), S. 15–20

[15] Becker, S. ; Urbassek, H. ; Horsch, M. ; Hasse, H.: Contact Angle of Sessile Drops in Lennard-Jones Systems. In: Langmuir 30 (2014), S. 13606–13614

[16] Yan, P. ; Rong, Y. ; Wang, G.: The Effect of Cutting Fluids Applied in Metal Cutting Process. In: J. Engineering Manufacture 230 (2016), S. 19–37

[17] Allen, M. ; Tildesley, D.: Computer Simulations of Liquids. Oxford: Clarendon Press, 1987

[18] Karniadakis, G. ; Beskok, A. ; Aluru, N.: Microflows and Nanoflows. Bd. Second Edition. New York : Springer-Verlag, 2005

[19] Zhen, S. ; Davies, G.: Lennard-Jones n-m Potential Energy Parameters. In: Phys. Stat. Sol. 78 (1983), S. 595

[20] Kelchner, C. ; Plimpton, S. ; Hamilton, J.: Dislocation Nucleation and Defect Structure During Surface Indentation. In: Phys. Rev. B 58 (1998), S. 11085–11088

[21] Plimpton, S.: Fast Parallel Algorithms for Short-Range Molecular Dynamics. In: J. Comp. Phys. 117 (1995), S. 1–19. – 17.11.2016

[22] Childs, T.: Friction Modelling in Metal Cutting. In: Wear 260 (2006), S. 310–318

[23] Vrabec, J. ; Kedia, G. ; Fuchs, G. ; Hasse, H.: Comprehensive Study of the Vapour–liquid Coexistence of the Truncated and Shifted Lennard–Jones Fluid Including Planar and Spherical Interface Properties. In: Molecular Physics 104 (2006), S. 1509–1527

[24] Vo, T. ; Park, B. ; Park, C. ; Kim, B.: Nano-Scale Liquid Film Sheared Between Strong Wetting Surfaces: Effects of Interface Region on the Flow. In: J. Mech. Sc. Tech. 29 (2015), S. 1681–1688

[25] Edelbrunner, H. ; Mücke, E.: Three-dimensional Alpha Shapes. In: ACM Trans Graph 12 (1994), S. 43–72

[26] Hess, S. ; Kröger, M. ; Fischer, P.: Einfache und disperse Flüssigkeiten In: Gase, Nanosysteme, Flüssigkeiten, Bergmann-Schaefer, Lehrbuch der Experimentalphysik. Vol 5. Berlin: W. de Gruyter, 2005, S. 385-468

[27] Younglove, B.: Thermophysical Properties of Fluids. I. Argon, Ethylene, Parahydrogen, Nitrogen, Nitrogen Trifluoride, and Oxygen. In: J. Phys. Chem. Ref. Data 11 (1982) S. 356

[28] Belak, J. ; Stowers, I.: A Molecular Dynamics Model of Orthogonal Cutting Process. In: Proc. Am. Soc. Precis. Eng. Annu. Conf. (1990), S. 76–79.

[29] Kapitza, P.: The Study of Heat Transfer in Helium II. In: J. Phys. (USSR) 4 (1941), S. 181-210

[30] Kim, B. ; Bestok, A. ; Cagin, T.: Molecular Dynamics Simulations of

Thermal Resistance at the Liquid-Solid Interface. In: J. Chem. Phys. 129 (2008), S. 174701

[31] Shi, Z. ; Barisik, M. ; Bestok, A.: Molecular Dynamics Modeling of Thermal Resistance at Argon-Graphite and Argon-Silver Interfaces. In: Int. J. Therm. Sc. 59 (2012), S. 29-37

[32] Kaburaki, H. ; Li, J. ; Yip, S. ; Kimizuka, H.: Dynamical Thermal Conductivity of Argon Crystal. In: J. Appl. Phys. 102 (2007), S. 043514

[33] Sun, J. ; Wang, W. ; Wang, H.: Viscous Dissipation Effect in Nano-confined Shear Flows: A Comparative Study Between Molecular Dynamics and Multi-scale Hybrid Simulations. In: Microfluidics and Nanofluidics 18 (2015), S. 103-109